Long-term and high frequency non-destructive monitoring of water stable isotope profiles in an evaporating soil column

Y. Rothfuss[1], S. Merz[1], J. Vanderborght[1], N. Hermes[1], A. Weuthen[1], A. Pohlmeier[1], H. Vereecken[1] and N. Brüggemann[1]

[1]{Forschungszentrum Jülich GmbH, Institute of Bio- and Geosciences, Agrosphere Institute (IBG-3), Leo-Brandt-Straße, D-52425 Jülich, Germany}

Correspondence to: Y. Rothfuss (y.rothfuss@fz-juelich.de)

Abstract

The stable isotope compositions of soil water (δ^2H and δ^{18}O) carry important information about the prevailing soil hydrological conditions and for constraining ecosystem water budgets. However, they are highly dynamic, especially during and after precipitation events. In this study, we present an application of a method based on gas-permeable tubing and isotope-specific infrared laser absorption spectroscopy for *in situ* determination of δ^2H and δ^{18}O. We conducted a laboratory experiment where a sand column was initially saturated, exposed to evaporation for a period of 290 days, and finally rewatered. Soil water vapor δ^2H and δ^{18}O were measured daily at each of eight available depths. Soil liquid water δ^2H and δ^{18}O were inferred from those of the vapor assuming thermodynamic equilibrium between liquid and vapor phases in the soil. The experimental setup allowed following the evolution of soil water δ^2H and δ^{18}O profiles with a daily temporal resolution. As the soil dried, we could also show for the first time the increasing influence of the isotopically depleted ambient water vapor on the isotopically enriched liquid water close to the soil surface (i.e., atmospheric invasion). Rewatering at the end of the experiment led to instantaneous resetting of the stable isotope profiles, which could be closely followed with the new method.

From simple soil δ^2H and δ^{18}O gradients calculations, we showed that the gathered data allowed to determinate the depth of the Evaporation Front (EF) and how it receded into the soil overtime. It was inferred that after 290 days under the prevailing experimental conditions,

the EF had moved down to an approximate depth of –0.06 m. Finally, data was used to calculate evaporation lines' slopes and test the formulation for isotope kinetic effects. A very good agreement was found between measured and simulated values (Nash and Sutcliffe Efficiency - NSE = 0.92) during the first half of the experiment, i.e., until the EF reached a depth of –0.04 m. From this point, calculated kinetic effects associated with the transport of isotopologues in the soil surface air layer above the EF provided slopes lower than observed. Finally, values of isotope kinetic effects that provided the best model-to-data fit (NSE > 0.9) were obtained from inverse modelling, highlighting uncertainties associated with the determinations of isotope kinetic fractionation and soil relative humidity at the EF.

1   Introduction

Stable isotopologues of water, namely $^1H^2H^{16}O$ and $^1H_2^{18}O$ are powerful tools used in a wide range of research disciplines at different and complementary temporal and spatial scales. They provide ways of assessing the origin of water vapor (e.g., Craig, 1961; Liu et al., 2010), solving water balances of lakes (Jasechko et al., 2013) and studying groundwater recharge (Blasch and Bryson, 2007; Peng et al., 2014). Analysis of the isotope compositions (δ^2H and $\delta^{18}O$) of soil surface and leaf waters allows for partitioning evapotranspiration into evaporation and transpiration (e.g., Dubbert et al., 2013; Hu et al., 2014; Rothfuss et al., 2012; Yepez et al., 2005).

Moreover, from soil water δ^2H and $\delta^{18}O$ profiles, it is also possible to derive quantitative information, such as soil evaporation flux, locate evaporation fronts, and root water uptake depths (Rothfuss et al., 2010; Wang et al., 2010). Zimmermann et al. (1967) and later Barnes and Allison (1983, 1984) and Barnes and Walker (1989) first analytically described soil $^1H^2H^{16}O$ and $^1H_2^{18}O$ movement at steady / non-steady state and in isothermal/ non-isothermal soil profiles. Between precipitation events, the soil water δ^2H and $\delta^{18}O$ profiles depend on flux boundary conditions, i.e., fractionating evaporation and non-fractionating capillary rise as well as on soil properties (e.g., soil tortuosity). In a saturated soil, the isotope excess at the surface due to evaporation diffuses back downwards, leading to typical and well documented exponential-shaped δ^2H and $\delta^{18}O$ profiles. For an unsaturated soil, assuming in a first approximation that isotope movement occurs in the vapor phase above the soil "evaporation front" (EF) and strictly in the liquid phase below it, the maximal δ^2H and $\delta^{18}O$ values are no longer observed at the surface but at the depth of EF. Above the EF, in the so-called "vapor

region", according to Fick's law, soil water δ^2H and δ^{18}O decrease towards the depleted ambient atmosphere water vapor δ^2H and δ^{18}O. Braud et al. (2005), Haverd and Cuntz (2010), Rothfuss et al. (2012), Singleton et al. (2004), and Sutanto et al. (2012) implemented the description of the transport of ^{1}H^{2}H^{16}O and ^{1}H$_2$^{18}O in physically based soil-vegetation-atmosphere transfer (SVAT) models (HYDRUS 1D, SiSPAT-Isotope, Soil-Litter iso, TOUGHREACT). In these models, movement of soil ^{1}H^{2}H^{16}O and ^{1}H$_2$^{18}O occur in both phases below and above the EF, and heat and water transports are properly coupled.

However, these tools suffer from the comparison with other "traditional" methods developed to observe and derive soil water state and transport. In contrast with soil water content and tension measured by, e.g., time-domain reflectometry and tensiometry, isotope compositions of soil water are determined either following destructive sampling or non-destructively but with poor spatial and temporal resolution (i.e., with section cups in combination with lysimeters for soil water tension higher than −600 hPa, e.g., Goldsmith et al., 2011, Litaor, 1988). This greatly limits their informative value. Only since recently, non-destructive methodologies based on gas-permeable membrane and laser spectroscopy can be found in the literature (Rothfuss et al., 2013; Herbstritt et al., 2012; Volkmann and Weiler, 2014, Gaj et al., 2015).

The central objective of this study was to demonstrate that a direct application of the method of Rothfuss et al. (2013) to a soil column would allow monitoring soil water δ^2H and δ^{18}O profiles in the laboratory with high temporal resolution and over a long time period. We will demonstrate that the obtained isotope data can be used to locate the evaporation front as it recedes into the soil during the experiment. Finally, data will be also used to test the expression proposed by Gat (1971) and based on the Craig and Gordon (1965) of evaporation lines' slopes.

2   Material and methods

2.1   Isotopic analyses

Isotopic analysis of liquid water and water vapor was performed using a cavity ring-down spectrometer (L1102-i, Picarro, Inc., Santa Clara, CA, USA), calibrated against the international primary water isotope standards V-SMOW2, GISP, and SLAP by liquid water injection into the vaporizer of the analyzer. Primary and working standards' isotope

compositions were measured at 17,000 ppmv water vapor mixing ratio (number of replicates = 4, number of injections per replicate = 8). Mean values and standard deviations were calculated omitting the first three values of the first replicate to account for a potential memory effect of the laser spectrometer. The laser spectrometer's dependence on water vapor mixing ratio was also investigated according to the method of Schmidt et al. (2010). Hydrogen and oxygen isotope ratios of water are expressed in per mil (‰) on the international "delta" scale as defined by Gonfiantini (1978) and referred to as δ^2H and δ^{18}O, respectively.

2.2 Soil column and measurements

The experiment was conducted in a 0.0057 m^3 acrylic glass column (0.11 m inside diameter, 0.60 m height, Fig. 1a). The bottom of the column consisted of a porous glass plate (10 10^{-6} m < pore size diameter < 16 10^{-6} m (4th class), Robu® GmbH, Hattert, Germany) connected to a two-way manual valve (VHK2-01S-06F, SMC Pneumatik GmbH, Germany).

Three ports were available at each of eight different depths (–0.01, –0.03, –0.05, –0.07, –0.10, –0.20, –0.40, and –0.60 m): one inlet for the carrier gas, i.e., synthetic dry air (20.5 % O_2 in N_2, with approx. 20-30 ppmv water vapor; Air Liquide, Germany), one sample air outlet, and one duct for a soil temperature (T_S) sensor (type K thermocouple, Greisinger electronic GmbH, Regenstauf, Germany; precision: 0.1°C). An additional fourth port at depths –0.01, –0.03, –0.05, –0.10, –0.20, and –0.60 m was used for the measurement of soil volumetric water content (θ) (EC-5, Decagon Devices, USA; precision: 0.02 m^3 m^{-3}).

At each depth inside the column a 0.15 m long piece of microporous polypropylene tubing (Accurel® PP V8/2HF, Membrana GmbH, Germany; 1.55 10^{-3} m wall thickness, 5.5 10^{-3} m inside diameter, 8.6 $10^{\wedge-3}$ m outside diameter) was connected to the gas inlet and outlet port. The tubing offers the two advantages of being gas-permeable (pore size of 0.2 10^{-6} m) and exhibiting strong hydrophobic properties to prevent liquid water from intruding into the tubing. It allows sampling of soil water vapor and, hence, the determination of the isotope composition of soil liquid water (δ_{Sliq}) in a non-destructive manner considering thermodynamic equilibrium between liquid and vapor phases as detailed by Rothfuss et al. (2013).

2.3 Internal isotope standards

Two internal standards ("st1" and "st2") were prepared using the same procedure as described by Rothfuss et al. (2013). Two closed acrylic glass vessels (0.122 m i.d., 0.22 m height), in each of which a 0.15 meter long piece of tubing as well as a type K thermocouple were installed, were filled with FH31 sand (porosity = 0.34 m^3 m^{-3}, dry bulk density = 1.69 10^3 kg m^3, particle size distribution: 10% (> 0.5 10^{-3} m), 72% (0.25 - 0.5 10^{-3} m), and 18% (< 0.25 10^{-3} m)) (Merz et al., 2014; Stingaciu et al., 2009). Each vessel was saturated with water of two different isotope compositions: δ^2H_{st1} = −53.51 (± 0.10) ‰, $\delta^{18}O_{st1}$ = −8.18 (± 0.06) ‰ and δ^2H_{st2} = +15.56 (± 0.12) ‰, $\delta^{18}O_{st2}$ = +8.37 (± 0.04) ‰). Soil water vapor from each vessel was sampled eight times per day for 30 min during the whole experiment.

2.4 Atmospheric measurements

Laboratory air was sampled passively with a 1/8" three meter-long stainless steel tubing at 2 m above the sand surface for isotope analysis of water vapor (δ_a). Air relative humidity (rh) and temperature (T_a) were monitored at the same height with a combined rh and T_a sensor (RFT-2, UMS GmbH, Germany; precision for rh and T_a were 2 % and 0.1°C, respectively). Vapor pressure deficit (vpd) was calculated from rh and T_a data using the Magnus-Tetens formula (Murray, 1967) for saturated vapor pressure. The laboratory was air-conditioned and ventilated with seven axial fans (ETRI 148VK0281, 117 l s^{-1} airflow, ETRI/Rosenberg, USA) positioned at 1.80 m height above the sand surface.

2.5 Sampling protocol and applied isotopic calibrations

The column was filled in a single step with FH31 sand and carefully shaken in order to reach a dry bulk density close to *in situ* field conditions. The sand was then slowly saturated from the bottom from an external water tank filled with st1 water on December 2, 2013. After saturation, the column was disconnected and sealed at the bottom using the two-way manual valve. It was finally installed on a balance (Miras 2 − 60EDL, Sartorius, USA), and let to evaporate for a period of 290 days in a ventilated laboratory.

δ_{Sliq} was determined in a sequential manner at each available depth once a day following the method developed by Rothfuss et al. (2013) (Fig. 1b). Dry synthetic air at a rate of 50 ml min^{-1} from a mass flow controller (EL-FLOW Analog, Bronkhorst High Tech, Ruurlo, The Netherlands) was directed to the permeable tubing for 30 minutes at each depth. The sampled

soil water vapor was diluted with dry synthetic air provided by a second mass flow controller of the same type. This allowed (i) reaching a water vapor mixing ratio ranging between 17,000 and 23,000 ppmv (where L1102-i isotope measurements are most precise) and (ii) generating an excess flow downstream of the laser analyser. By doing this, any contamination of sample air with ambient air would be avoided. The excess flow was measured with a digital flow meter (ADM3000, Agilent Technologies, Santa Clara, CA, USA). The last 100 observations (corresponding to approx. 10 minutes) at steady state (standard deviations <0.70 ‰ and <0.20 ‰ for δ^2H and δ^{18}O, respectively) were used to calculate the raw isotope compositions of soil water vapor (δ_{Svap}). The latter was corrected for the water vapor mixing ratio dependence of the laser analyzer readings with 17,000 ppmv as reference level. Measurements that did not fulfil the above mentioned conditions for δ^2H and δ^{18}O standard deviations were not taken into account. Finally, these corrected values were used to infer the corresponding δ_{Sliq} at the measured T_S (Eq. (1) and (2); taken from Rothfuss et al., 2013):

$$\delta^2 H_{Sliq} = 104.96 - 1.0342 \cdot T_S + 1.0724 \cdot \delta^2 H_{Svap} \qquad (1)$$

$$\delta^{18} O_{Sliq} = 11.45 - 0.0795 \cdot T_S + 1.0012 \cdot \delta^{18} O_{Svap} \qquad (2)$$

The isotope composition of laboratory water vapor (δ_a) was measured eight times a day. δ_a, δ_{Svap}, and δ_{Sliq} values were finally corrected for laser instrument drift with time, using the isotope compositions of the two water standards, δ_{st1} and δ_{st2}.

Water vapor of the ambient air, of both standards, and from the different tubing sections in the soil column were sampled sequentially in the following order: soil (0.60 m) – soil (0.40 m) – atmosphere – st1 – st2 – soil (0.20 m) – soil (0.10 m) – atmosphere – st1 – st2 – soil (0.07 m) – soil (0.05 m) – atmosphere – st1 – st2 – soil (0.03 m) – soil (0.01 m). Atmosphere water vapor was sampled twice as long (i.e., one hour) as soil water vapor from the column/standards so that each sequence lasted exactly 10 hours and started each day at the same time. The remaining 14 hours were used for additional standard and atmosphere water vapor measurements (i.e., on five occasions each).

2.6 Irrigation event

On Day of Experiment (DoE) 290 at 09:30 the sand surface was irrigated with 70 mm of st1 water. This was achieved over one hour in order to avoid oversaturation of the sand and avoid preferential pathways that would have affected the evaporation rate. For this, a 2 L

1 polyethylene bottle was used. Its bottom was perforated with a set of 17 holes of 5 mm

2 diameter and its cap with a single hole through which a PTFE bulkhead union tube fitting

3 (Swagelok, USA) was installed. The bulkhead fitting was connected to a two-way needle

4 valve (Swagelok, USA). Opening/closing the valve controlled the flow rate at which air

5 entered the bottle headspace, which in turn controlled the irrigation flow rate.

6 To better observe the dynamics directly following the irrigation event, water vapor was

7 sampled at a higher rate, i.e., 1, 3, 4, 5, 6, 9, 11, and 11 times per day at –0.60, –0.40, –0.20, –

8 0.10, –0.07, –0.05, –0.03, and –0.01 m. Water vapor from both standards was sampled twice a

9 day. The experiment was terminated after 299 days on September 26th, 2014.

10 ## 2.7 Evaporation lines

11 Gat et al. (1971) proposed an expression based on the model of Craig and Gordon (1965) for

12 the slope of the so-called "evaporation line" (S_{Ev}, [-]) which quantifies the relative change in

13 $\delta^2 H_{Sliq}$ and $\delta^{18} O_{Sliq}$ in a water body undergoing evaporation:

14 $$S_{Ev} = \frac{\Delta\left(\delta^2 H_{Sliq}\right)}{\Delta\left(\delta^{18} O_{Sliq}\right)} = \frac{\left[rh\cdot\left(\delta_a - \delta_{Sliq\_ini}\right) + \varepsilon_{eq} + \Delta\varepsilon\right]_{^2H}}{\left[rh\cdot\left(\delta_a - \delta_{Sliq\_ini}\right) + \varepsilon_{eq} + \Delta\varepsilon\right]_{^{18}O}} \qquad (3)$$

15 with δ_{Sliq_ini} the initial soil water (hydrogen or oxygen) liquid isotope composition, i.e., prior

16 removal of water vapor by fractionating evaporation. ε_{eq} [-, expressed in ‰] is the

17 equilibrium enrichment in either $^1H^2H^{16}O$ or $^1H_2{}^{18}O$. It is defined by the deviation from unity

18 of the ratio between water and isotopologue saturated vapor pressures and can be calculated

19 using the empirical closed-form equations proposed by, e.g., Majoube (1971). $\Delta\varepsilon$ [-,

20 expressed in ‰] is the so-called "isotope kinetic effect" associated with $^1H^2H^{16}O$ and $^1H_2{}^{18}O$

21 vapor transports. Assuming that (i) turbulent transport is a non-fractionating process and

22 considering that (ii) the ratio of molecular diffusion resistance to total resistance equals one, it

23 follows that (Gat, 2000):

24 $$\Delta\varepsilon = (1 - rh)\cdot\left(\frac{D^v}{D_i^v} - 1\right)\cdot n \qquad (4)$$

1   In Equation (4), the product $\left(\dfrac{D^v}{D_i^v}-1\right)\cdot n$ is the isotope kinetic enrichment (ε_K, [-, expressed in

2   ‰]). In the present study, values for ratios of diffusivities (D^v/D_i^v) were taken from Merlivat

3   (1978):

4   $$\begin{cases} \dfrac{D^v}{D^v_{^2H}} = 0.9755 \\[2mm] \dfrac{D^v}{D^v_{^{18}O}} = 0.9723 \end{cases} \qquad \text{(5a and 5b)}$$

5   The term n accounts for the aerodynamic in the air boundary layer and ranges from $n_a = 0.5$

6   (turbulent diffusion, i.e., atmosphere-controlled conditions) to $n_S = 1$ (molecular diffusion,

7   i.e., soil-controlled conditions) with a value of ⅔ corresponding to laminar flow conditions

8   (Dongmann et al., 1974, Brutsaert, 1975). We tested the formulation proposed by Mathieu

9   and Bariac (1996) where n is considered as a function of soil water content:

10   $$n = \frac{\left(\theta_{surf}-\theta_{res}\right)\cdot n_a + \left(\theta_{sat}-\theta_{res}\right)\cdot n_S}{\theta_{sat}-\theta_{res}} \qquad \text{(6)}$$

11   with θ_{res}, θ_{sat}, and θ_{surf} the residual, saturated and surface soil water contents [$m^3\ m^{-3}$].

12   Note that Equation (3) contrasts with the expression for the slope characterizing equilibrium

13   processes (e.g., precipitation formation) and therefore strictly temperature-dependant (i.e.,

14   $S_{eq} = \varepsilon_{eq}^{^2H} / \varepsilon_{eq}^{^{18}O}$). While S_{eq} might range for instance from 7.99 to 8.94 (for temperatures

15   spanning between 5 and 30°C), a much wider spread in S_{Ev} values is possible and has been

16   measured between 2 and 6 (Barnes and Allison, 1988, Brunel et al., 1995, DePaolo et al.,

17   2004).

18   **3   Results**

19   **3.1   Example of a measuring sequence**

20   Figure 2 shows exemplarily the measuring sequence for DoE 150. Soil and standards water

21   vapor mixing ratios were stable and ranged from 17,200 to 18,200 ppmv during the last 10

22   minutes of each sampling period (Fig. 2a). δ_{Svap} was within the range spanned by δ_{st1vap} and

23   δ_{st2vap} for both ^2H and ^{18}O (Fig. 2b). On DoE 150, the soil surface was sufficiently dry so that

24   atmospheric invasion of water vapor had started to significantly influence the δ_{Svap} of the

1 upper soil layers. Therefore, δ_{Svap} measured at –0.01 m was lower than at –0.03 m for both ^{2}H

2 and ^{18}O, but less pronounced for ^{2}H.

3.2 Time courses of air temperature, relative humidity and atmospheric δ^2H and δ^{18}O

5 During the experiment, the laboratory air temperature ranged from 15.6 to 22.5 °C (average:

6 18.7 ± 1.5 °C, Fig. 3a) and the relative humidity from 19 to 69 % (average: 40 % ± 0.08 %,

7 Fig. 3a). Lower values of δ_a were observed from DoE 0 to 125 at lower air temperatures,

8 whereas higher values occurred after DoE 125 at higher air temperatures (Fig. 3b).

3.3 Evolution of soil water content, temperature, evaporation flux, and δ_{Svap} from DoE 0-290

11 The soil temperature ranged from 16.2 to 22.3 °C (average: 18.6 ± 1.3 °C, data not shown)

12 and closely followed that in the air, i.e., differences between daily mean soil and air

13 temperatures ranged from -0.2 to 0.2 °C during the experiment. Following the saturation of

14 the column, a strong decrease in water content was observed in the upper 10 cm, whereas

15 after 287 days the sand was still saturated at –0.60 m (Fig. 4a). Figure 4b shows the time

16 series of evaporation flux normalized by the vapor pressure deficit in the laboratory air

17 (*Ev/vpd*, expressed in mm day^{-1} kPa^{-1}). *Ev/vpd* ratio was high at the beginning of the

18 experiment, i.e., ranged from 2.44 to 3.22 mm d^{-1} kPa^{-1} during the first two experimental

19 days. After DoE 180 and until the soil was irrigated, *Ev/vpd* stabilized to a mean value of 0.03

20 (±0.02) mm d^{-1} kPa^{-1}.

21 Due to fractionating evaporation flux, the δ_{Svap} of the topmost layer (–0.01 m) increased

22 instantaneously (i.e., from DoE 0 onward) from the equilibrium δ_{Svap} value with the input

23 water (–17.3 ‰ and –132.3 ‰ for ^{18}O and ^{2}H, respectively, at 16.5°C, Fig. 4c and d).

24 Through back-diffusion of the excess heavy stable isotopologues from the evaporation front,

25 δ_{Svap} measured at depths –0.03, –0.05, –0.07, –0.10, and –0.20 m departed from that same

26 equilibrium value after 2, 3, 10, 25, and 92 days of the experiment, respectively. On the other

27 hand, δ_{Svap} of the layers –0.40 and –0.60 m were constant over the entire duration of the

28 experiment. Until DoE 65, the δ_{Svap} of the first 10 cm increased. From DoE 65 to 113 δ_{Svap}

29 reached an overall stable value in the top layers –0.01 m (δ^2H$_{Svap}$ = 4.82 ± 2.06 ‰; δ^{18}O$_{Svap}$ =

30 11.72 ± 0.67 ‰) and –0.03 m (δ^2H$_{Svap}$ = 5.61 ± 3.14 ‰; δ^{18}O$_{Svap}$ = 10.41 ±0.81 ‰), whereas

1   δ_{Svap} measured at depths –0.05, –0.07, and –0.10 m still progressively increased; from DoE 72

2   onward, δ_{Svap} at –0.20 m started to increase. δ^2H_{Svap} and $\delta^{18}O_{Svap}$ values started to decrease

3   after about DoE 113 and DoE 155, respectively. δ^2H_{Svap} at –0.01, –0.03, and –0.07 m on the

4   one hand and $\delta^{18}O_{Svap}$ at –0.01, –0.03, and –0.07 m on the other followed similar evolutions

5   with maximum values measured below the surface down to –0.05 m.

3.4   Evolution of soil water content, temperature, evaporation flux, and δ_{Svap} from DoE 290 to 299

8   The layers –0.01, –0.03, –0.05, –0.10, and –0.20 m showed increases in θ of 0.31, 0.22, 0.30,

9   0.23, and 0.16 m^3 m^{-3} following irrigation, whereas θ at –0.60 m remained constant (Fig. 4e).

10    $\theta_{-0.01m}$ and $\theta_{-0.03m}$ rapidly decreased down to values of 0.12 and 0.13 m^3 m^{-3}. Note that when

11    $\theta_{-0.01m}$ and $\theta_{-0.03m}$ reached these values prior to irrigation, the evaporation rate was similar

12   (i.e., $Ev/vpd = 0.65$ (±0.12) mm d^{-1}, Fig. 4f).

13   Immediately after irrigation and for both isotopologues, δ_{Svap} at –0.01, –0.03, and –0.05 m

14   was reset to a value close to that in equilibrium with st1 water (i.e., –17.8 ‰ and –132.0 ‰

15   for ^{18}O and ^2H, respectively, at 21.8 °C soil temperature, Fig. 4g and h). At –0.07 m, δ_{Svap}

16   reached the above mentioned equilibrium values after about 3.5 days. δ_{Svap} at –0.20 m evolved

17   in a similar way, whereas at –0.10 m the equilibrium values were reached after six hours.

18   Finally, δ_{Svap} at –0.40 and –0.60 m and for both isotopologues were not affected by the water

19   addition, which was consistent with the observed θ changes.

3.5   Evolution of soil temperature, water content, and δ_{Sliq} profiles

21   In Figure 5, T_S, θ, and δ_{Sliq} profiles for both isotopologues are plotted in three different panels,

22   from DoE 0 to 100 (Fig. 5a-d, top panels), from DoE 101 to 287 (Fig. 5e-h, center panels),

23   and from DoE 288 to 299 (Fig. 5i-l, bottom panels). The represented profiles were obtained

24   from a linear interpolation of the times series of each variable. Thus, since the measuring

25   sequence started each day at 08:00 and ended at 18:00, the depicted profiles are centered on

26   13:00.

27   Even if the soil temperature fluctuated during the course of the experiment, quasi-isothermal

28   conditions were fulfilled at a given date, as the column was not isolated from its surroundings.

29   On average, T_S only varied by 0.2 °C around the profile mean temperature at a given date.

30   The δ_{Sliq} profiles showed a typical exponential shape from DoE 0 to approx. 100. Around DoE

1   100, when θ at –0.01 m reached a value of 0.090 m^3 m^{-3} (i.e., significantly greater than the

2   sand residual water content $\theta = 0.035$ m^3 m^{-3}, determined by Merz et al. (2014)), the maximal

3   δ_{Sliq} values were no longer observed at the surface and atmosphere water vapor started

4   invading the first centimeter of soil. Note that this happened slightly faster for $^1H^2H^{16}O$ than

5   for $^1H_2^{18}O$. On DoE 290, when the column was irrigated, the isotope profiles were partly reset

6   to their initial state, i.e., constant over depth and close to –53.5 and –8.2 ‰ for $^1H^2H^{16}O$ and

7    $^1H_2^{18}O$, respectively, with the exception of still enriched values at –0.07 m.

8   **3.6 δ^2H-δ^{18}O relationships in soil water and atmosphere water vapor**

9   Each plot of Figure 6 represents data of 50 consecutive days of the experiment. Laboratory

10   atmosphere water vapor δ^2H and δ^{18}O (gray symbols) were linearly correlated (linear

11   regression relationships in gray dotted lines) during the entire experiment (R^2 ranging

12   between 0.74 and 0.90, F-statistic p-value < 0.01), with the exception of the period DoE 125-

13   155 (R$^2 = 0.31$, p < 0.001), when atmospheric water vapor δ^2H was remarkably high in the

14   laboratory (Fig. 6c and d).

15   The linear regression slopes (LRS) between δ^2H_a and $\delta^{18}O_a$ ranged from 6.20 (DoE 50-100, p

16   < 0.01) to 8.29 (DoE 0-50, gray dotted line, p < 0.001). These values were significantly lower

17   than S_{eq}, the calculated ratio between the liquid-vapor equilibrium fractionations of $^1H^2H^{16}O$

18   and $^1H_2^{18}O$ (Majoube, 1971) that characterizes meteoric water bodies, which should have

19   ranged from 8.41 to 8.92 at the measured monthly mean atmosphere temperatures

20   (Forschungszentrum Jülich wheater station, 6°24'34" E, 50°54'36" N, 91 m.a.s.l.). Therefore,

21   it can be deduced that the laboratory air moisture was partly resulting from column

22   evaporation, typically leading to a δ^2H-δ^{18}O regression slope of lower than eight. This also

23   highlights the particular experimental conditions in the laboratory, where other sources of

24   water vapor (e.g., by opening the laboratory door) might have influenced the isotope

25   compositions of the air.

26   Considering all soil depths, the δ^2H_{Sliq}-$\delta^{18}O_{Sliq}$ LRS increased from 2.96 to 4.86 over the

27   course of the experiment (with R$^2 > 0.89$, p < 0.001). These values were much lower than that

28   of the slope of the Global Meteoric Water Line (GMWL, i.e., slope=8) also represented in

29   Figure 6. However, Figure 6 highlights the fact that in the upper three layers (–0.01, –0.03,

30   and –0.05 m) δ^2H_{Sliq}-$\delta^{18}O_{Sliq}$ LRS followed a significantly different evolution as the soil dried

31   out. Figure 7 shows average δ^2H-δ^{18}O LRS calculated for time intervals of ten consecutive

days for the atmosphere (gray line), the three upper layers (colored solid lines), and the remaining deeper layers (–0.07, –0.10, –0.20, –0.40, and –0.60 m, black dotted line). While both δ^2H-δ^{18}O LRS in the atmosphere and in the first three depths fluctuated during the experiment, the LRS of the combined remaining deeper layers varied only little between 3.07 and 4.49 (average = 3.78 ± 0.54). From DoE 150, δ^2H-δ^{18}O LRS of the atmosphere and at – 0.01, –0.03, and –0.05 m were linearly correlated (R^2 = 0.73, 0.48, and 0.42, with p < 0.001, < 0.01, and < 0.05, respectively), whereas they were not correlated before DoE 125, demonstrating again the increasing influence of the atmosphere (atmosphere invasion) on the soil surface layer as the EF receded in the soil. Note the negative δ^2H$_a$-δ^{18}O$_a$ LRS (R^2 = 0.26, p < 0.001) observed between DoE 125 and 150, due to remarkably high atmosphere vapor δ^2H measured in the laboratory.

4 Discussion

4.1 Long term reliability of the method

The method proved to be reliable in the long term as the tubing sections positioned at –0.60 and –0.40 m (i.e., where the sand was saturated or close to saturation during the entire experiment) remained watertight even after 299 days. As demonstrated by Rothfuss et al. (2013), (i) the length of the gas-permeable tubing, (ii) the low synthetic dry air flow rate, and (iii) the daily measurement frequency allowed removing soil water vapor which remained under thermodynamic equilibrium with the soil moisture. Moreover, this was also true for the upper soil layers even at low soil water content: steady values for water vapor mixing ratio and isotope compositions were always reached during sampling throughout the experiment. Finally, our method enabled inferring the isotope composition of tightly bound water at the surface. This would be observable by the traditional vacuum distillation method with certainly a lower vertical resolution due to low moisture content. As also pointed out by Rothfuss et al. (2013), it can be assumed that the sand properties did not cause any fractionation of pore water ^{2}H and ^{18}O. In contrast, this could not be the case in certain soils with high cation exchange capacity (CEC) as originally described by Sofer and Gat (1972) and recently investigated by Oerter et al. (2014).

4.2 Locating the evaporation front depth from soil water δ^2H and δ^{18}O profiles

From Figure 4b no distinct characteristic evaporation stages, i.e., stages I and II referring to atmosphere-controlled and soil-controlled evaporation phases, respectively, could be identified. The opposite was observed by Merz et al. (2014), who conducted an evaporation study using the same sand. This indicates greater wind velocity in the air layer above the soil column due to the laboratory ventilation. For higher wind velocities, the boundary layer above the drying medium is thinner and the transfer resistance for vapor transfer lower than for lower wind velocities. But, for thinner boundary layers, the evaporation rates depends stronger on the spatial configuration of the vapor field above the partially wet evaporating surface. This makes that the evaporation rate decreases and the transfer resistance in the boundary layer increases more in relative terms with decreasing water content of the evaporation surface for higher than for lower wind velocities (Shahraeeni et al., 2012).

Locating the EF in the soil is of importance for evapotranspiration partitioning purposes: from the soil water isotope composition at the EF, it is possible to calculate the evaporation flux isotope composition using the Craig and Gordon formula (Craig and Gordon, 1965). For a uniform isotope diffusion coefficient distribution in the liquid phase, an exponential decrease of the isotope composition gradient with depth is expected. However, when evaporation and thus accumulation of isotopologues occur in a soil layer between two given observation points, then the isotope gradient between these two points is smaller than the gradient deeper in the profile. Therefore we can consider the time when the isotope composition gradient is no longer the largest between these two upper observation depths as the time when the EF moves into the soil layer below.

Figure 8a and b display the evolutions of the isotope compositions gradients $d\left(\delta^{18}O_S\right)/dz$ and $d\left(\delta^2H_S\right)/dz$ calculated between two consecutive observation points in the soil (i.e., between –0.01 and –0.03 m in brown solid line, between –0.03 and –0.05 m in red solid line, etc.). Figure 8c translates these isotope gradients in terms of EF depths ($z^{18}O_{EF}$ and z^2H_{EF}, respectively). Each day, the maximum $d\left(\delta^{18}O_S\right)/dz$ and $d\left(\delta^2H_S\right)/dz$ define the layer where evaporation occurs, e.g., when $d\left(\delta^{18}O_S\right)/dz$ is maximal between –0.01 and –0.03 m on a given DoE, $z^{18}O_{EF}$ is estimated to be greater than –0.01 m and is assigned the value of 0 m. When $d\left(\delta^{18}O_S\right)/dz$ is maximal between –0.03 and –0.05 m on a given DoE, $z^{18}O_{EF}$ is estimated to range between–0.01 and –0.03 m and is assigned the value –0.02 m. From

13

1 both $d\left(\delta^{18}O_S\right)/dz$ and $d\left(\delta^2H_S\right)/dz$, a similar evolution of the depth of the evaporation front

2 was derived despite the fact that δ^2H_{Sliq} and $\delta^{18}O_{Sliq}$ time courses were different and showed

3 maxima at different times. It was inferred that after 290 days under the prevailing laboratory

4 air temperature, moisture, and aerodynamic conditions, and given the specific hydraulic

5 properties of the sand, the EF had moved down to an approximate depth of –0.06 m.

6 ## 4.3 Isotope kinetic effects during soil evaporation

7 For each period of ten consecutive days the minimum measured δ^2H_{Sliq} and $\delta^{18}O_{Sliq}$ provided

8 $\delta^2H_{Sliq\_ini}$ and $\delta^{18}O_{Sliq\_ini}$ in Equation (3). δ^2H_a and $\delta^{18}O_a$ were obtained from the mean values

9 of their respective times series. Mean soil surface water content (θ_{surf}) measured in the layer

10 above the EF (as identified in section 4.2) provided the n parameter in Equation (6) and

11 ultimately ε_K^{2H} and ε_K^{18O} (Eq. (5a) and (5b)). ε_{eq}^{2H} and ε_{eq}^{18O} were calculated from Majoube (1971)

12 at the mean soil temperature measured at z_{EF}. Relative humidity was normalized to the soil

13 temperature measured at the EF. Finally, standard error for S_{Ev} was obtained using an

14 extension of the formula proposed by Phillips and Gregg (2001) and detailed by Rothfuss et

15 al. (2010). For this, standard errors associated with the determination of the variables in

16 Equation (3) were taken equal to their measured standard deviations for each time period.

17 Standard errors for the parameters θ_{res} and θ_{sat} were set to 0.01 m^3 m^{-3} (i.e., comparable to the

18 soil water content probes' precision) and for the diffusivity ratios D/D^{2H} and D/D^{18O} to zero

19 (i.e., no uncertainty about their value was taken into account, although debatable, e.g., Cappa

20 et al., 2003).

21 Figure 9a shows the comparison between time courses of S_{Ev} and δ^2H_{Sliq}-$\delta^{18}O_{Sliq}$ LRS

22 computed with data below the EF. Both ranged between 2.9 and 4.8, i.e., within the range of

23 reported values (e.g., Barnes and Allison, 1988, Brunel et al., 1995, DePaolo et al., 2004).

24 Note that both observed and simulated slopes' values increased over time, even though the air

25 layer above the EF gradually thickened as the soil dried out. The opposite was observed by

26 e.g., Barnes and Allison (1983), who simulated isotopic profiles at steady state with constant

27 relative humidity. In the present study however the atmosphere relative humidity gradually

28 increased which in turn decreased the kinetic effects associated with $^1H^2H^{16}O$ and $^1H_2^{18}O$

29 vapor transports and thus increased slopes over time. The general observed trend was very

30 well reproduced by the model between DoE 30 and 150 (Nash and Sutcliffe Efficiency - NSE

31 = 0.92; Nash and Sutcliffe, 1970), whereas S_{Ev} departed from data from DoE 150 onwards

(NSE < 0). Overall, the Craig and Gordon (1965) model could explain about 62 % of the data variability with a Root Mean Square Error (RMSE) of 0.58 (and 76 % when data from the period DoE 0-10 is left out, p-value < 0.001, RMSE = 0.52). At the beginning of the experiment (DoE 0-20), simulated values were greater than computed δ^2H-δ^{18}O LRS, even when taking into account the high S_{Ev} standard errors due to fast changing θ_{surf} (Phillips and Gregg, 2001). Although S_{Ev} was equal to 3.8 for the period DoE 0-10, δ^2H-δ^{18}O LRS had already reached down a value of 2.9, meaning that the EF should have been no longer at the surface (i.e., between the surface and 0.01 m depth) leading to greater n, therefore lower slope value.

After DoE 150 and until DoE 290 when evaporation flux was lower than 0.40 mm d^{-1}, difference between model and data progressively increased. For a better model-to-data fit, the ^{1}H^{2}H^{16}O and ^{1}H$_2$^{18}O kinetic effects should decrease, through either (i) decrease of n, which is from a theoretical point of view counter-intuitive and e.g., contradicts the formulation of Mathieu and Bariac (1996) or (ii) decrease of term $(1 - rh)$, or else (iii) a combination of (i) and (ii). In another laboratory study where δ^{18}O of water in bare soil columns was measured destructively and δ^{18}O of evaporation was estimated from cryoscopic trapping of water vapor at the outlet of the columns' headspaces, Braud et al. (2009a and b) could capture ε_K^{18o} dynamics by inverse modelling. In their case, ε_K^{18o} generally reached values close to $\varepsilon_K^{18o} = 18.9$‰ corresponding to laminar conditions above the liquid-vapor interface (n = 2/3). They however determined at the end of their experiments, when the soil surface dry layer thickened and soil surface relative humidity was significantly lower than 100%, values lower than reported in the literature (i.e., $\varepsilon_K^{18o} < 14.1$‰). These results were partly explained by the particular experimental conditions leading to uncertainties in characterizing evaporation isotope compositions when the dry soil surface layer was the most developed. Nevertheless, the same observation could be made in the present study while having a different soil texture (silt loam *versus* quartz sand) and noticeable different atmospheric conditions ("free" laboratory atmosphere *versus* sealed headspace circulated with dry air). Figure 9c displays the evolution of ε_K^{2H} (resp. ε_K^{18o}) that provided the best fit with data (NSE = 0.99) through fitting of the n parameter (shown Figure 9b) instead of calculating it with Equation (6). In this scenario, n decreased from one to 0.59, with a mean value of 0.96 ± 0.03 during the period DoE 0-150.

1 Instead of changing the value of n over time (and therefore those of $\varepsilon_K^{2_H}$ and $\varepsilon_K^{18_O}$), another

2 possibility is to consider that after some time the relative humidity at the EF (rh_{EF}) was

3 different from 100%, although the EF was still at thermodynamic equilibrium. In that case

4 kinetic effects would have depended on the difference ($rh_{EF} - rh$) instead of ($1 - rh$). Figure

5 9b shows the rh_{EF} time course that provided the best model-to-data fit (NSE = 0.92), when

6 $\varepsilon_K^{2_H}$ and $\varepsilon_K^{18_O}$ were calculated (Eq. (5a-5b-6)). In this second scenario, rh_{EF} decreased from 100

7 to 81 % with a mean value of 99.5 ± 0.03 % for the period DoE 0-150, i.e., in a similar

8 fashion than fitted n values obtained in the 1st scenario. These values were significantly lower

9 than what is calculated with Kelvin's Equation linking rh_{EF} with soil water tension at the EF

10 in the case of liquid-vapor equilibrium, which for the soil retention properties (Merz et al.,

11 2014) would range between 100 and 99.6 %. In a third scenario one could consider a

12 combined decrease of n and rh_{EF} to smaller extents, for which there are no unique solutions at

13 each time step. In a fourth scenario, the ratio of turbulent diffusion resistance to molecular

14 diffusion resistance is no more negligible, leading to n' values ranging between 0 and n

15 (Merlivat and Jouzel, 1979). This last scenario was however not verifiable. In any case, only

16 decreasing kinetic effects could provide a better model-to-data fit. Note that the formulation

17 of kinetic enrichments proposed by Merlivat and Coantic (1975) and based on the evaporation

18 model of Brutsaert (1982) was not tested due to lack of appropriate data (i.e., unknown wind

19 distribution profile over the soil column). The formulations of Melayah et al. (1996) (n = 0)

20 and Barnes and Allison (1983) (n = 1) were also not tested as they give kinetic enrichments

21 constant over time and cannot explain a change of S_{Ev} value through change of n. Finally, S_{Ev}

22 calculations using diffusivity ratios determined by Cappa et al. (2003) lead to lower value of

23 S_{Ev} and less good model-to-data fit.

24 In the present study, information on δ^2H and $\delta^{18}O$ of the evaporation flux was missing to

25 address uncertainties in the determination of $\varepsilon_K^{2_H}$ and $\varepsilon_K^{18_O}$. The experimental setup would also

26 have gained from the addition of appropriate sensors (e.g., micro-psychrometers) to measure

27 the soil surface relative humidity and especially rh_{EF}, although the dimensions of the column

28 would certainly be a limiting factor. A more in depth investigation of the behavior of S_{Ev} (and

29 isotope composition gradients with depth for that matter) with time could be carried out with

30 detailed numerical simulations using an isotope-enabled SVAT model such as SiSPAT-

31 Isotope.

5   Conclusion

Since the initial work of Zimmermann et al. (1967), water stable isotopologues have proven both theoretically and experimentally to be valuable tools for the study of water flow in the soil and at the soil-atmosphere interface. In this work we present the first application of the method of Rothfuss et al. (2013). This study constitutes also the very first long-term application of the series of newly developed isotopic monitoring systems based on gas-permeable tubing and isotope-specific infrared laser absorption spectroscopy (Herbstritt et al., 2012; Volkmann and Weiler, 2014).Our method proved to be reliable over long time periods and followed quantitatively the progressive isotope enrichment caused by evaporation in an initially saturated soil column. Moreover, it could capture sudden variations following a simulated intense rain event.

Simple calculations of isotope compositions' gradients made it possible to evaluate the position of the Evaporation Front and observe how it progressively receded with time in the soil. Confrontation of the model of Craig and Gordon (1965) with data also highlighted uncertainties associated with the determinations of isotope kinetic fractionations and soil relative humidity at the EF when the soil surface dry layer was the most developed and evaporation flux was low.

Our method will allow experimentalists to measure and locate the evaporation front in a dynamic and non-destructive manner and to calculate the isotope compositions of the evaporation flux using the model of Craig and Gordon (1965) with much higher time resolution. Provided that the isotope compositions of evapotranspiration and transpiration fluxes are measured or modelled, this method will be especially useful to test hypotheses and improve our understanding of root water uptake processes and the partitioning of evapotranspiration fluxes.

3

References

Barnes, C. J., and Allison, G. B.: The Distribution of Deuterium and O-18 in Dry Soils .1. Theory, J. Hydrol., 60, 141-156, doi: 10.1016/0022-1694(83)90018-5, 1983.

Barnes, C. J., and Allison, G. B.: The Distribution of Deuterium and O-18 in Dry Soils .3. Theory for Non-Isothermal Water-Movement, J. Hydrol., 74, 119-135, doi: 10.1016/0022-1694(84)90144-6, 1984.

Barnes, C. J., and Allison, G. B.: Tracing of water movement in the unsaturated zone using stable isotopes of hydrogen and oxygen, J. Hydrol., 100, 143–176, doi:10.1016/0022-1694(88)90184-9, 1988

Barnes, C. J., and Walker, G. R.: The Distribution of Deuterium and O-18 during Unsteady Evaporation from a Dry Soil, J. Hydrol., 112, 55-67, doi: 10.1016/0022-1694(89)90180-7, 1989.

Blasch, K. W., and Bryson, J. R.: Distinguishing sources of ground water recharge by using delta H-2 and delta O-18, Ground Water, 45, 294-308, doi: 10.1111/j.1745-6584.2006.00289.x, 2007.

Braud, I., Bariac, T., Gaudet, J. P., and Vauclin, M.: SiSPAT-Isotope, a coupled heat, water and stable isotope (HDO and (H2O)-O-18) transport model for bare soil. Part I. Model description and first verifications, J. Hydrol., 309, 277-300, doi: 10.1016/j.jhydrol.2004.12.013, 2005.

Braud, I., Biron, P., Bariac, T., Richard, P., Canale, L., Gaudet, J. P., and Vauclin, M.: Isotopic composition of bare soil evaporated water vapor. Part I: RUBIC IV experimental setup and results, J. Hydrol., 369, 1-16, DOI 10.1016/j.jhydrol.2009.01.034, 2009a.

Braud, I., Bariac, T., Biron, P., and Vauclin, M.: Isotopic composition of bare soil evaporated water vapor. Part II: Modeling of RUBIC IV experimental results, J. Hydrol., 369, 17-29, DOI 10.1016/j.jhydrol.2009.01.038, 2009b.

Brunel, J. P., Walker, G. R, and Kennettsmith, A. K.: Field Validation of Isotopic Procedures for Determining Sources of Water Used by Plants in a Semiarid Environment, J. Hydrol., 167, 351-368, doi: 10.1016/0022-1694(94)02575-V, 1995.

1 Brutsaert, W.: A theory for local evaporation (or heat transfer) from rough and smooth
2 surfaces at ground level, Water Resour. Res., 11, 543-550, doi: 10.1029/WR011i004p00543,
3 1975.

4 Craig, H.: Isotopic Variations in Meteoric Waters, Science, 133, 1702-1703, doi:
5 10.1126/science.133.3465.1702, 1961.

6 Craig, H., and Gordon, L. I.: Deuterium and oxygen 18 variations in the ocean and marine
7 atmosphere, Stable Isotopes in Oceanographic Studies and Paleotemperatures, Spoleto, Italy,
8 1965, 9-130, 1965.

9 DePaolo, D. J., Conrad, M. E., Maher, K., and Gee, G. W.: Evaporation effects on oxygen and
10 hydrogen isotopes in deep vadose zone pore fluids at Hanford, Washington, Vad. Zone. J., 3,
11 220-232, doi:10.2113/3.1.220, 2004.

12 Dongmann, G., H. W. Nurnberg, H. Forstel, and Wagener, K.: Enrichment of $H_2^{18}O$ in
13 Leaves of Transpiring Plants, Radiat Environ Bioph, 1, 41-52, doi: 10.1007/Bf01323099,
14 1974.

15 Dubbert, M., Cuntz, M., Piayda, A., Maguás, C., and Werner, C.: Partitioning
16 evapotranspiration – Testing the Craig and Gordon model with field measurements of oxygen
17 isotope ratios of evaporative fluxes, J. Hydrol., 496, 142-153, doi:
18 10.1016/j.jhydrol.2013.05.033, 2013.

19 Gaj, M., Beyer, M., Koeniger, P., Wanke, H., Hamutoko, J., and Himmelsbach, T.: In-situ
20 unsaturated zone stable water isotope (^{2}H and ^{18}O) measurements in semi-arid environments
21 using tunable off-axis integrated cavity output spectroscopy, Hydrol. Earth Syst. Sci. Discuss.
22 12, 6115-6149, doi:10.5194/hessd-12-6115-2015, 2015.

23 Gat, J.: Comments on the Stable Isotope Method in Regional Groundwater Investigations,
24 Water Resour. Res., 7, 980-993, doi: 10.1029/WR007i004p00980, 1971

25 Gat, J. R.: Atmospheric water balance - the isotopic perspective, Hydrol. Process., 14, 1357-
26 1369, doi: 10.1002/1099-1085, 2000.

27 Goldsmith, G.R., Munoz-Villers, L.E., Holwerda, F., McDonnell, J.J., Asbjornsen, H.,
28 Dawson, T.E.: Stable isotopes reveal linkages among ecohydrological processes in a
29 seasonally dry tropical montane cloud forest, Ecohydrology, 5, 779-790, doi:
30 10.1002/eco.268, 2011.

1   Gonfiantini, R.: Standards for stable isotope measurements in natural compounds, Nature,

2   271, 534-536, doi: 10.1038/271534a0, 1978.

3   Haverd, V., and Cuntz, M.: Soil-Litter-Iso: A one-dimensional model for coupled transport of

4   heat, water and stable isotopes in soil with a litter layer and root extraction, J. Hydrol., 388,

5   438-455, doi: 10.1016/j.jhydrol.2010.05.029, 2010.

6   Herbstritt, B., Gralher, B., and Weiler, M.: Continuous in situ measurements of stable

7   isotopes in liquid water, Water Resour. Res., 48, doi: 10.1029/2011wr011369, 2012.

8   Hu, Z. M., Wen, X. F., Sun, X. M., Li, L. H., Yu, G. R., Lee, X. H., and Li, S. G.: Partitioning

9   of evapotranspiration through oxygen isotopic measurements of water pools and fluxes in a

10 temperate grassland, J Geophys Res-Biogeo, 119, 358-371, doi: 10.1002/2013jg002367,

11 2014.

12 Jasechko, S., Sharp, Z. D., Gibson, J. J., Birks, S. J., Yi, Y., and Fawcett, P. J.: Terrestrial

13 water fluxes dominated by transpiration, Nature, 496, 347-351, doi: 10.1038/Nature11983,

14 2013.

15 Litaor, M.I.: Review of Soil Solution Samplers. Water Resour. Res., 24, 727-733, doi:

16 10.1029/Wr024i005p00727, 1988

17 Liu, Z. F., Bowen, G. J., and Welker, J. M.: Atmospheric circulation is reflected in

18 precipitation isotope gradients over the conterminous United States, J. Geophys. Res.-Atmos.,

19 115, doi: 10.1029/2010jd014175, 2010.

20 Melayah, A., Bruckler, L., and Bariac, T.: Modeling the transport of water stable isotopes in

21 unsaturated sails under natural conditions .1. Theory, Water Resour. Res., 32, 2047-2054, doi:

22 10.1029/96wr00674, 1996.

23 Merlivat, L.: Molecular Diffusivities of H216O, HD16O, and H218O in Gases, J. Chem.

24 Phys., doi: 10.1063/1.436884, 1978

25 Merlivat, L., and Coantic, M.: Study of Mass-Transfer at Air-Water-Interface by an Isotopic

26 Method, J. Geophys. Res.-Oc. Atm., 80, 3455-3464, doi: 10.1029/Jc080i024p03455, 1975

27 Merlivat, L., and Jouzel, J.: Global Climatic Interpretation of the Deuterium-Oxygen-18

28 Relationship   for   Precipitation,   J   Geophys   Res-Oc   Atm,   84,   5029-5033,   doi:

29 10.1029/JC084iC08p05029, 1979.

Majoube, M.: Oxygen-18 and Deuterium Fractionation between Water and Steam, J. Chim. Phys. Phys.-Chim. Biol., 68, 1423-1436, 1971.

Mathieu, R., and Bariac, T.: A numerical model for the simulation of stable isotope profiles in drying soils, 101, 12685–12696, J. Geophys. Res.-Atmos., doi: 10.1029/96jd00223, 1996

Merz, S., Pohlmeier, A., Vanderborght, J., van Dusschoten, D., and Vereecken, H.: Moisture profiles of the upper soil layer during evaporation monitored by NMR, Water Resour. Res., 50, 5184-5195, doi: 10.1002/2013wr014809, 2014.

Murray, F. W.: On the Computation of Saturation Vapor Pressure, J. Appl. Meteorol., 6, 203-204, doi: 10.1175/1520-0450, 1967.

Nash, J. E., and Sutcliffe, J. V.: River flow forecasting through conceptual models part I -A discussion of principles, Journal of Hydrology, 10, 282-290, doi:10.1016/0022-1694(70)90255-6, 1970

Oerter, E., Finstad, K., Schaefer, J., Goldsmith, G. R., Dawson, T., and Amundson, R.: Oxygen isotope fractionation effects in soil water via interaction with cations (Mg, Ca, K, Na) adsorbed to phyllosilicate clay minerals, J. Hydrol., 515, 1-9, doi: 10.1016/j.jhydrol.2014.04.029, 2014.

Peng, T. R., Lu, W. C., Chen, K. Y., Zhan, W. J., and Liu, T. K.: Groundwater-recharge connectivity between a hills-and-plains' area of western Taiwan using water isotopes and electrical conductivity, J. Hydrol., 517, 226-235, doi: 10.1016/j.jhydrol.2014.05.010, 2014.

Phillips, D. L., and Gregg, J. W.: Uncertainty in source partitioning using stable isotopes, Oecologia, 127, 171-179, doi: 10.1007/s004420000578, 2001.

Rothfuss, Y., Biron, P., Braud, I., Canale, L., Durand, J. L., Gaudet, J. P., Richard, P., Vauclin, M., and Bariac, T.: Partitioning evapotranspiration fluxes into soil evaporation and plant transpiration using water stable isotopes under controlled conditions, Hydrol. Process., 24, 3177-3194, doi: 10.1002/Hyp.7743, 2010.

Rothfuss, Y., Braud, I., Le Moine, N., Biron, P., Durand, J. L., Vauclin, M., and Bariac, T.: Factors controlling the isotopic partitioning between soil evaporation and plant transpiration: Assessment using a multi-objective calibration of SiSPAT-Isotope under controlled conditions, J. Hydrol., 442, 75-88, doi: 10.1016/j.jhydrol.2012.03.041, 2012.

1   Rothfuss, Y., Vereecken, H., and Brüggemann, N.: Monitoring water stable isotopic
2   composition in soils using gas-permeable tubing and infrared laser absorption spectroscopy,
3   Water Resour. Res., 49, 1-9, doi: 10.1002/wrcr.20311, 2013.

4   Schmidt, M., Maseyk, K., Lett, C., Biron, P., Richard, P., Bariac, T., and Seibt, U.:
5   Concentration effects on laser-based d18O and d2H measurements and implications for the
6   calibration of vapour measurements with liquid standards, Rapid Commun. Mass Spectrom,
7   24, 3553–3561, doi: 10.1002/rcm.4813, 2010.

8   Shahraeeni, E., Lehmann, P., and Or, D.: Coupling of evaporative fluxes from drying porous
9   surfaces with air boundary layer: Characteristics of evaporation from discrete pores, Water
10   Resour. Res., 48, doi: 10.1029/2012wr011857, 2012.

11   Singleton, M. J., Sonnenthal, E. L., Conrad, M. E., DePaolo, D. J., and Gee, G. W.:
12   Multiphase reactive transport modeling of seasonal infiltration events and stable isotope
13   fractionation in unsaturated zone pore water and vapor at the Hanford site, Vadose Zone J., 3,
14   775-785, doi: 10.2113/3.3.775, 2004.

15   Sofer, Z., and Gat, J. R.: Activities and Concentrations of O-18 in Concentrated Aqueous Salt
16   Solutions - Analytical and Geophysical Implications, Earth Planet. Sc. Lett., 15, 232-&, doi:
17   10.1016/0012-821x(72)90168-9, 1972.

18   Stingaciu, L. R., Pohlmeier, A., Blumler, P., Weihermuller, L., van Dusschoten, D., Stapf, S.,
19   and Vereecken, H.: Characterization of unsaturated porous media by high-field and low-field
20   NMR relaxometry, Water Resour. Res., 45, doi: 10.1029/2008wr007459, 2009.

21   Sutanto, S. J., Wenninger, J., Coenders-Gerrits, A. M. J., and Uhlenbrook, S.: Partitioning of
22   evaporation into transpiration, soil evaporation and interception: a comparison between
23   isotope measurements and a HYDRUS-1D model, Hydrol. Earth Syst. Sc., 16, 2605-2616,
24   doi: 10.5194/hess-16-2605-2012, 2012.

25   Volkmann, T. H. M., and Weiler, M.: Continual in situ monitoring of pore water stable
26   isotopes in the subsurface, Hydrol. Earth Syst. Sc., 18, 1819-1833, doi: 10.5194/hess-18-
27   1819-2014, 2014.

28   Wang, P., Song, X. F., Han, D. M., Zhang, Y. H., and Liu, X.: A study of root water uptake of
29   crops indicated by hydrogen and oxygen stable isotopes: A case in Shanxi Province, China,
30   Agric. Water Manage., 97, 475-482, doi: 10.1016/j.agwat.2009.11.008, 2010.

1 Yepez, E. A., Huxman, T. E., Ignace, D. D., English, N. B., Weltzin, J. F., Castellanos, A. E., and Williams, D. G.: Dynamics of transpiration and evaporation following a moisture pulse in semiarid grassland: A chamber-based isotope method for partitioning flux components, Agr. Forest Meteorol., 132, 359-376, doi: 10.1016/j.agrformet.2005.09.006, 2005.

5 Zimmermann, U., Ehhalt, D., and Münnich, K. O.: Soil water movement and evapotranspiration: changes in the isotopic composition of the water, Symposium of Isotopes in Hydrology, Vienna, 1967, 567–584.
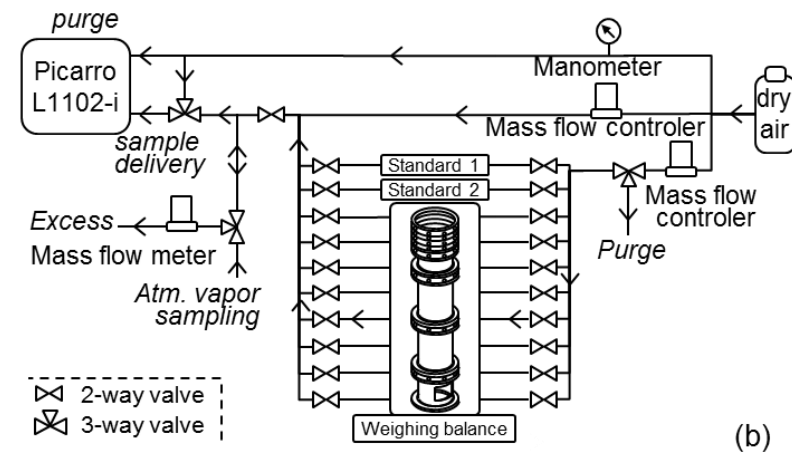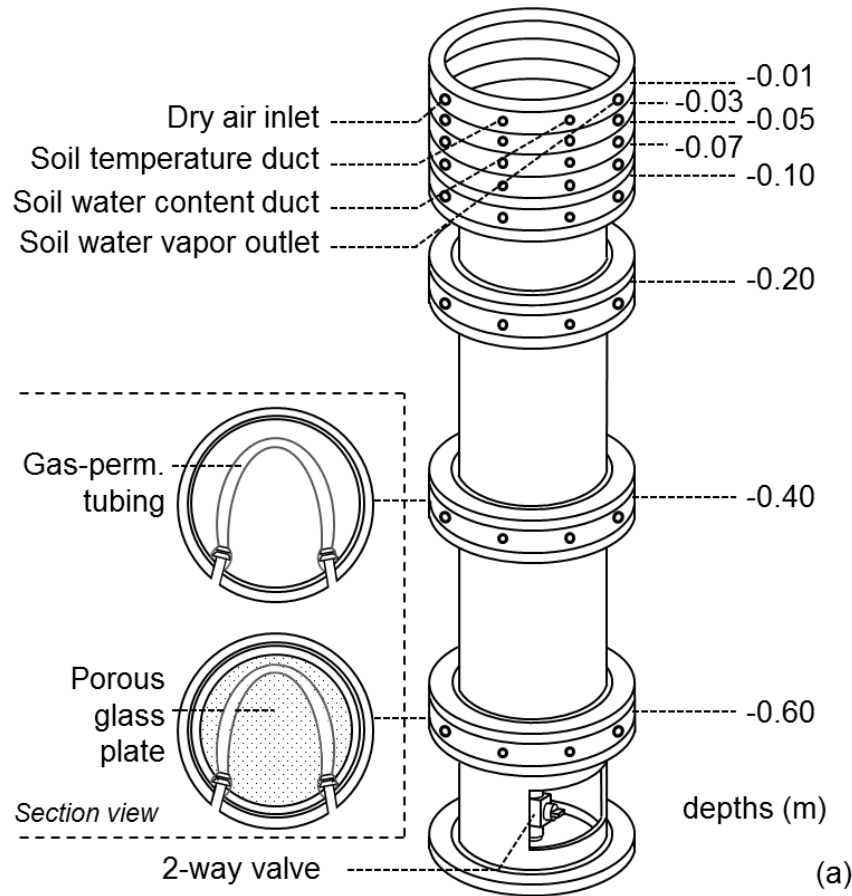
Figures

Figure 1. (a) Scheme of the acrylic glass column used in the experiment; (b) experimental setup for sampling water vapor at the different soil depths of the soil column, from the ambient air, and from the two soil water standards (standard 1 and 2)
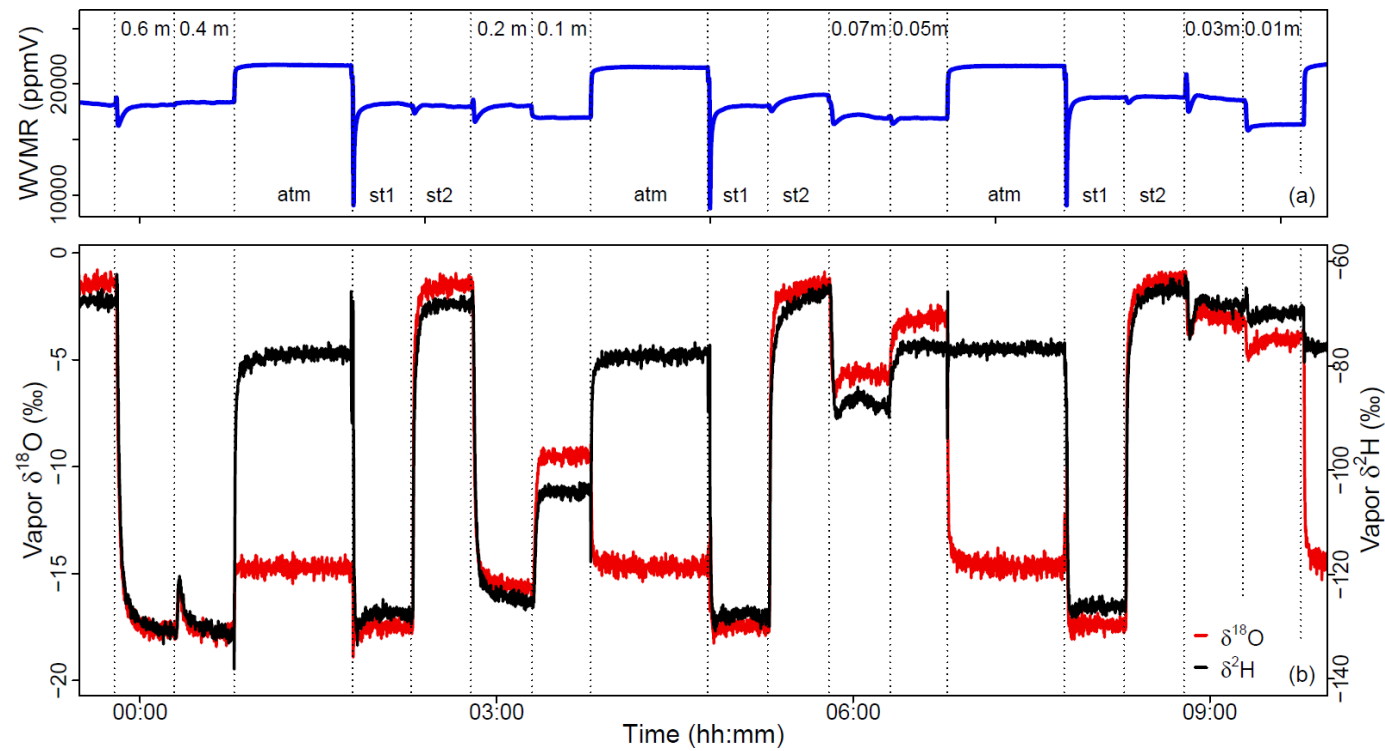
Figure 2. Water vapor mixing ratio (*WVMR*, in ppmv) and isotope composition ($\delta^{18}O$ and δ^2H, in ‰ V-SMOW) of the water vapor sampled on Day of Experiment 150 from the ambient air ("atm"), both standards ("st1" and "st2"), and from the tubing sections at soil depths 1, 3, 5, 7, 10, 20, 40, and 60 cm
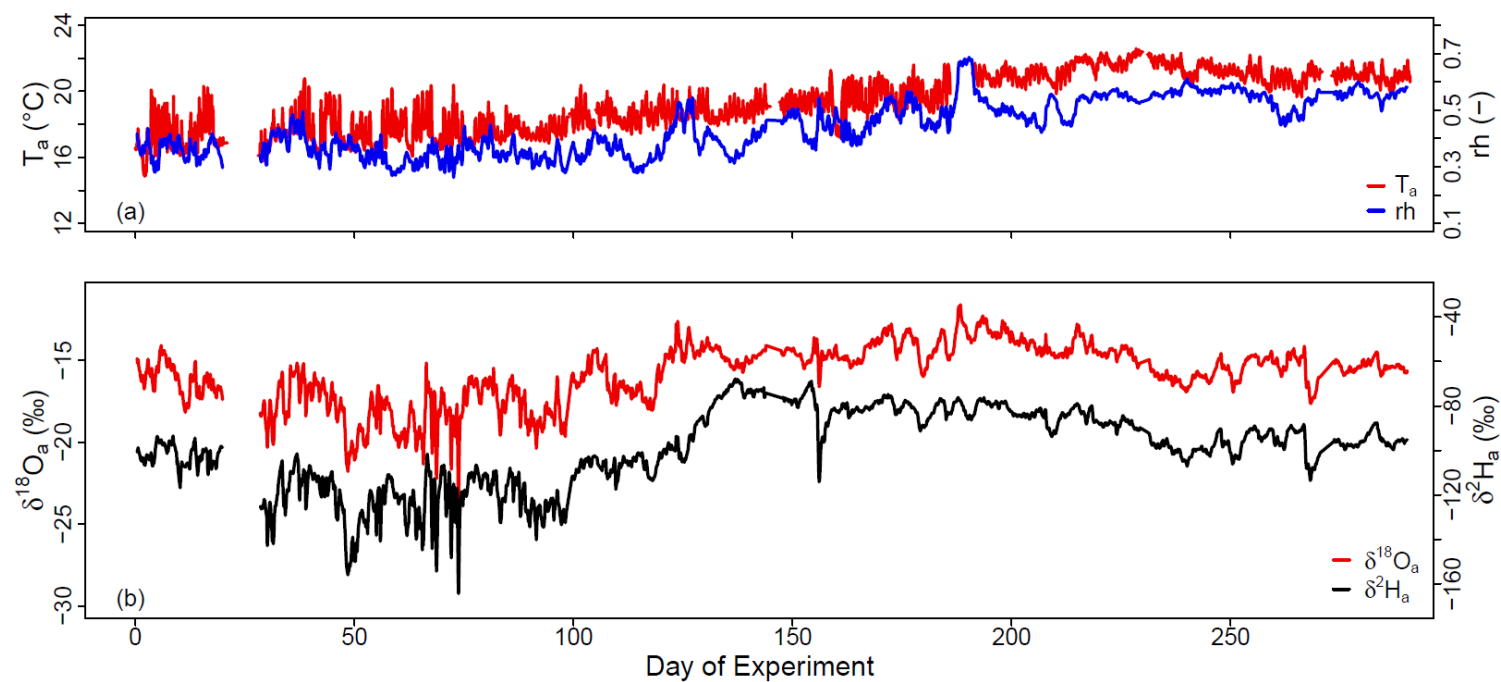
Figure 3. Time series of the laboratory ambient air temperature (T_a, in °C), relative humidity (rh, in %) and water vapor isotope compositions ($\delta^{18}O_a$ and δ^2H_a, in ‰ V-SMOW) over the course of the experiment
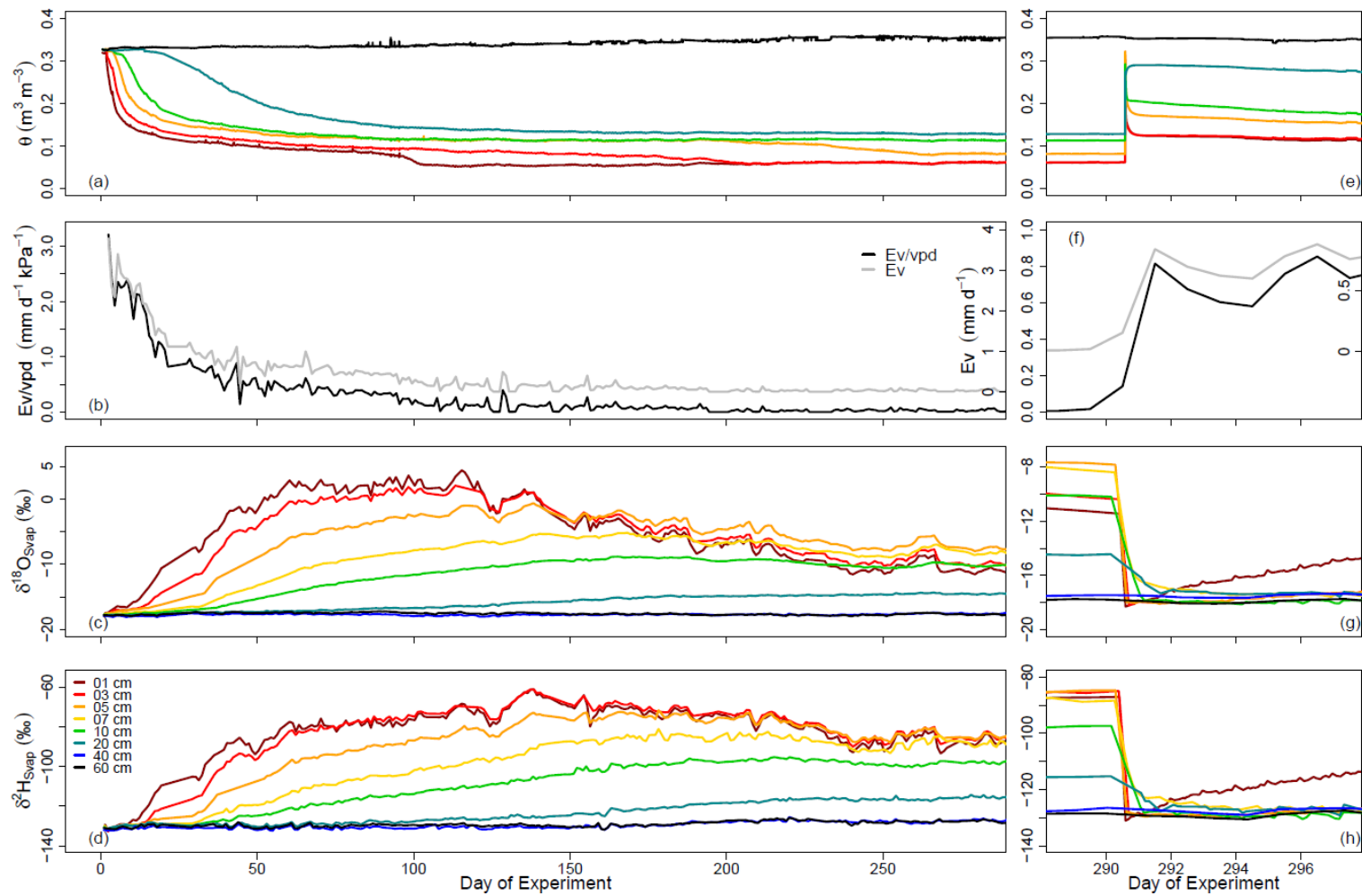
Figure 4. Time series of water content (θ, in m^3 m^{-3}), evaporation flux (Ev, in mm d^{-1}), and water vapor isotope compositions ($\delta^{18}O_{Svap}$ and δ^2H_{Svap}, in ‰ V-SMOW) during the course of the experiment
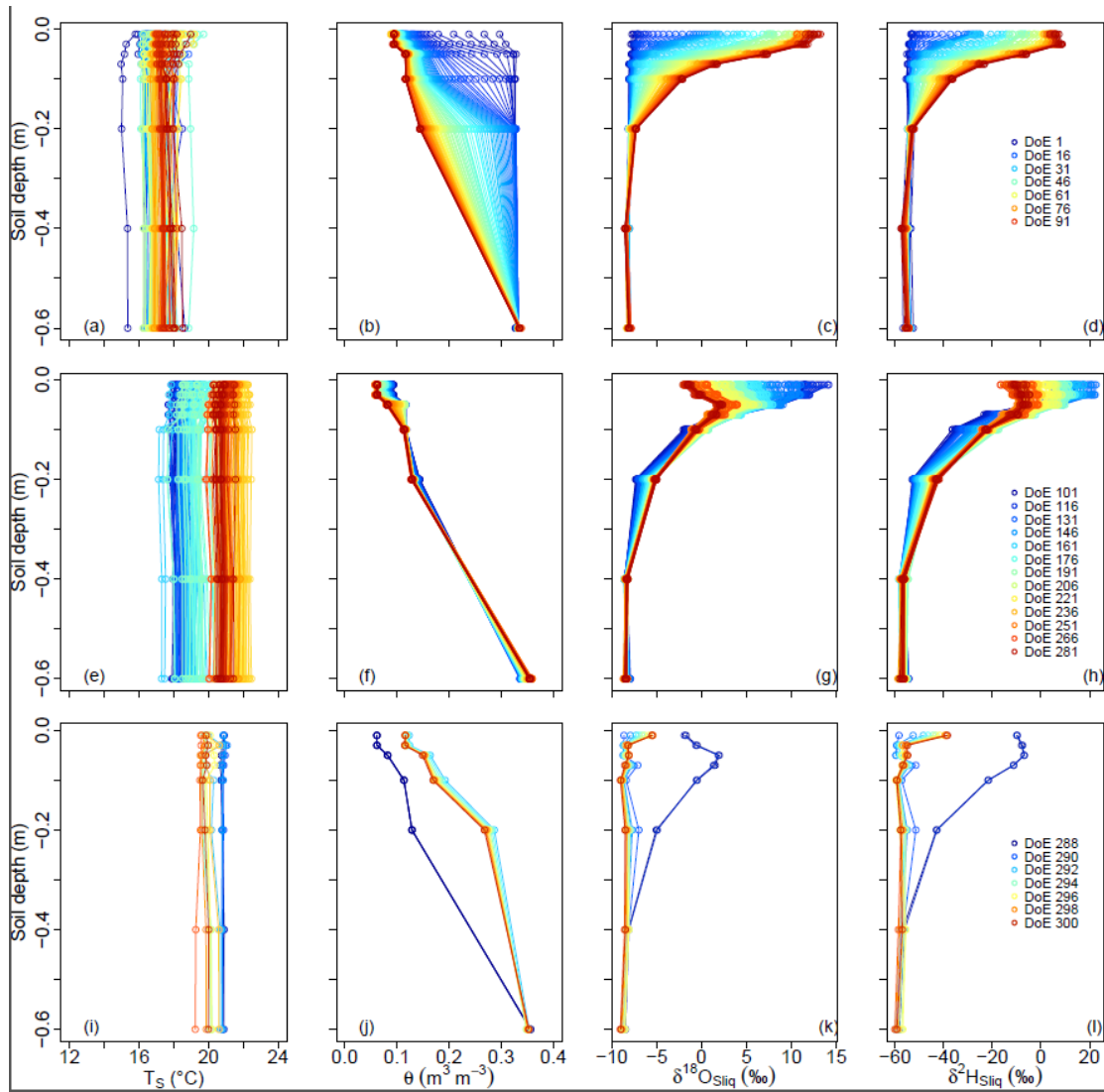
Figure 5. Soil temperature (T_S, in °C), water content (θ, in $m^3\ m^{-3}$), and liquid water isotope compositions ($\delta^{18}O_{Sliq}$ and δ^2H_{Sliq}, in ‰ V-SMOW) profiles from Day of Experiment (DoE) 0 - 100 (top panel), from DoE 101 - 287 (middle panel), and from DoE 288 - 299 (bottom panel)
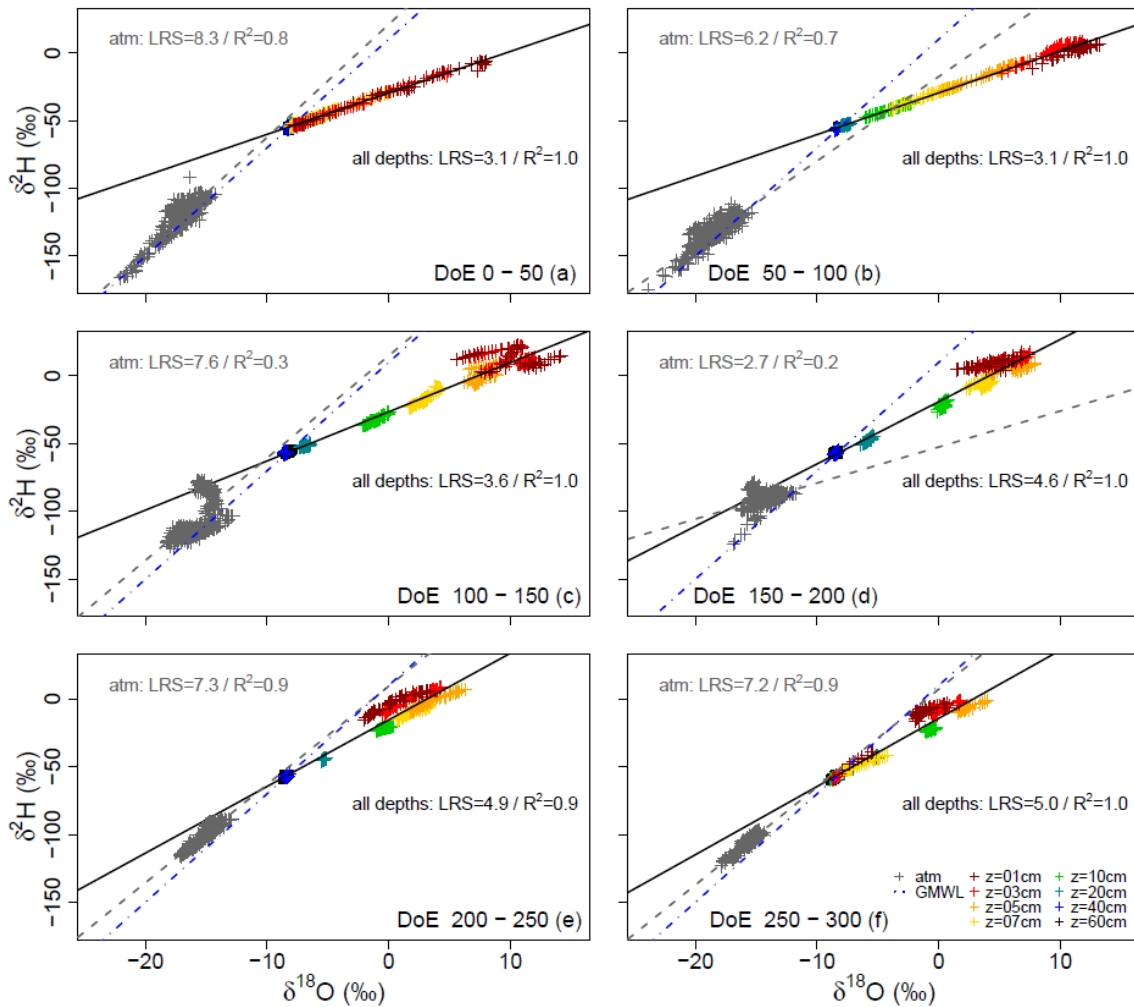
Figure 6. Linear regressions (gray dotted line) between laboratory atmosphere water vapor $\delta^{18}O$ and δ^2H (in ‰ V-SMOW) and between soil water $\delta^{18}O$ and δ^2H (solid black line). Each plot represents data from 50 consecutive days of experiment (DoE). Global Meteoric Water Line (GMWL, define by $\delta^2H = 8*\delta^{18}O + 10$, in blue dotted line) is shown on each sub-plot for comparison. Coefficient of determination (R^2) as well as the slope of the linear regressions (LRS) are reported

1
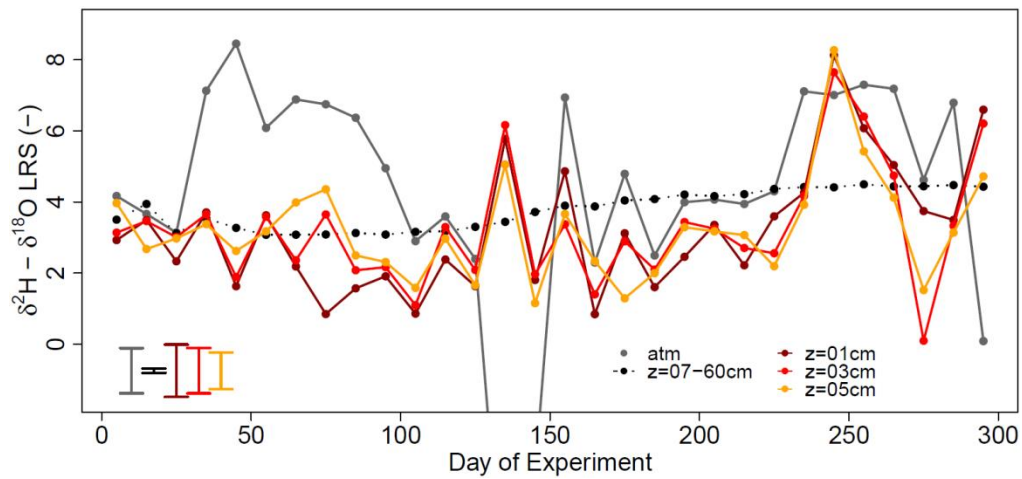
Figure 7. Time course of the slopes of the $\delta^{18}O$-δ^2H linear regressions (LRS) for time intervals of ten consecutive days of atmosphere data (gray solid line), soil data from the upper three layers (01, 03, and 05 cm, colored solid lines), and combined soil data from the remaining bottom layers (from 07 to 60 cm, black dotted line). Mean standard errors are represented by the error bars in the bottom left corner
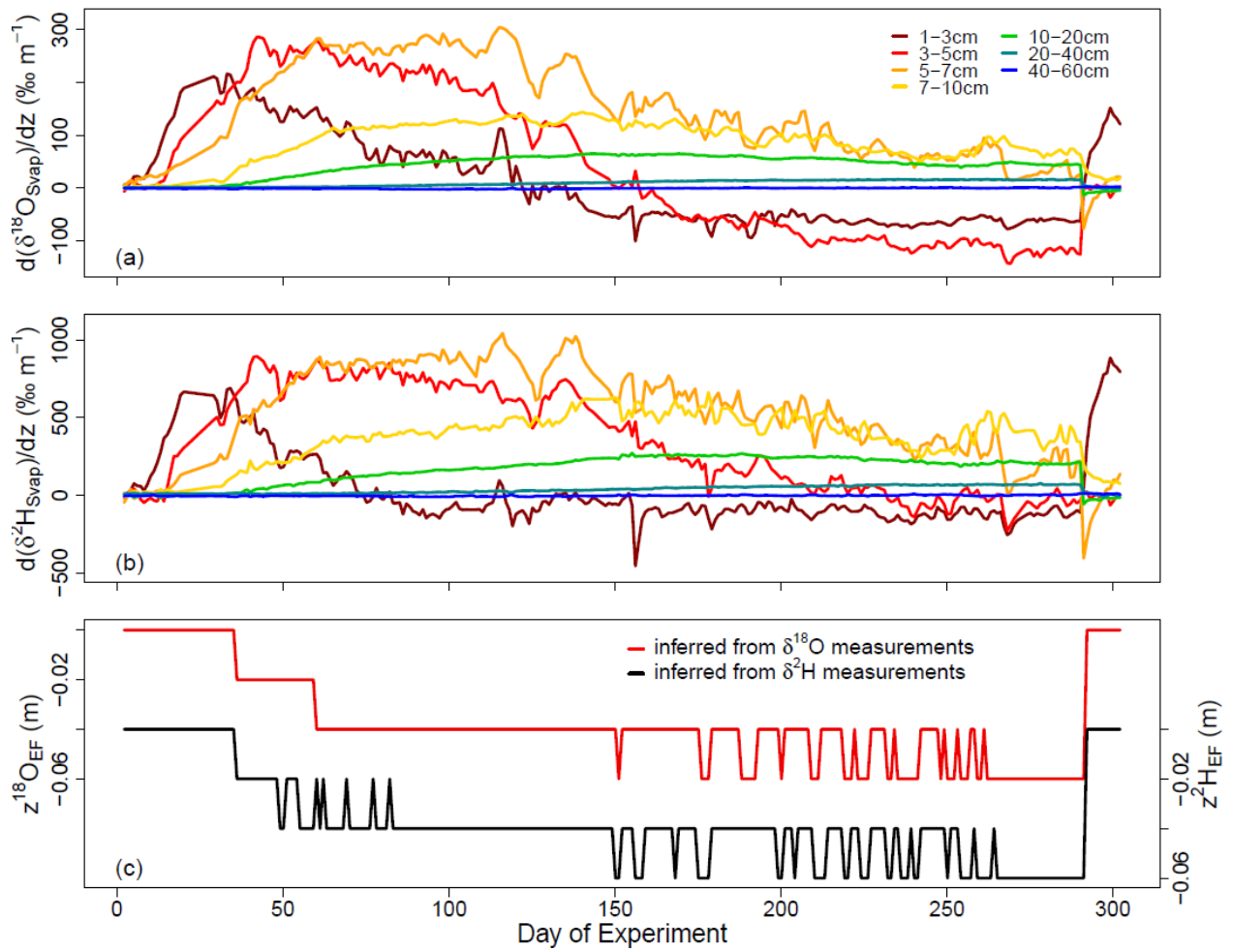
Figure 8. (a) and (b) $^1H^2H^{16}O$ and $^1H_2^{18}O$ composition gradients calculated between consecutive observation points in the soil. (c) Evolution of the evaporation front depths $z^{18}O_{EF}$ (red solid line) and z^2H_{EF} (black solid line) inferred from the $^1H^2H^{16}O$ and $^1H_2^{18}O$ composition gradients
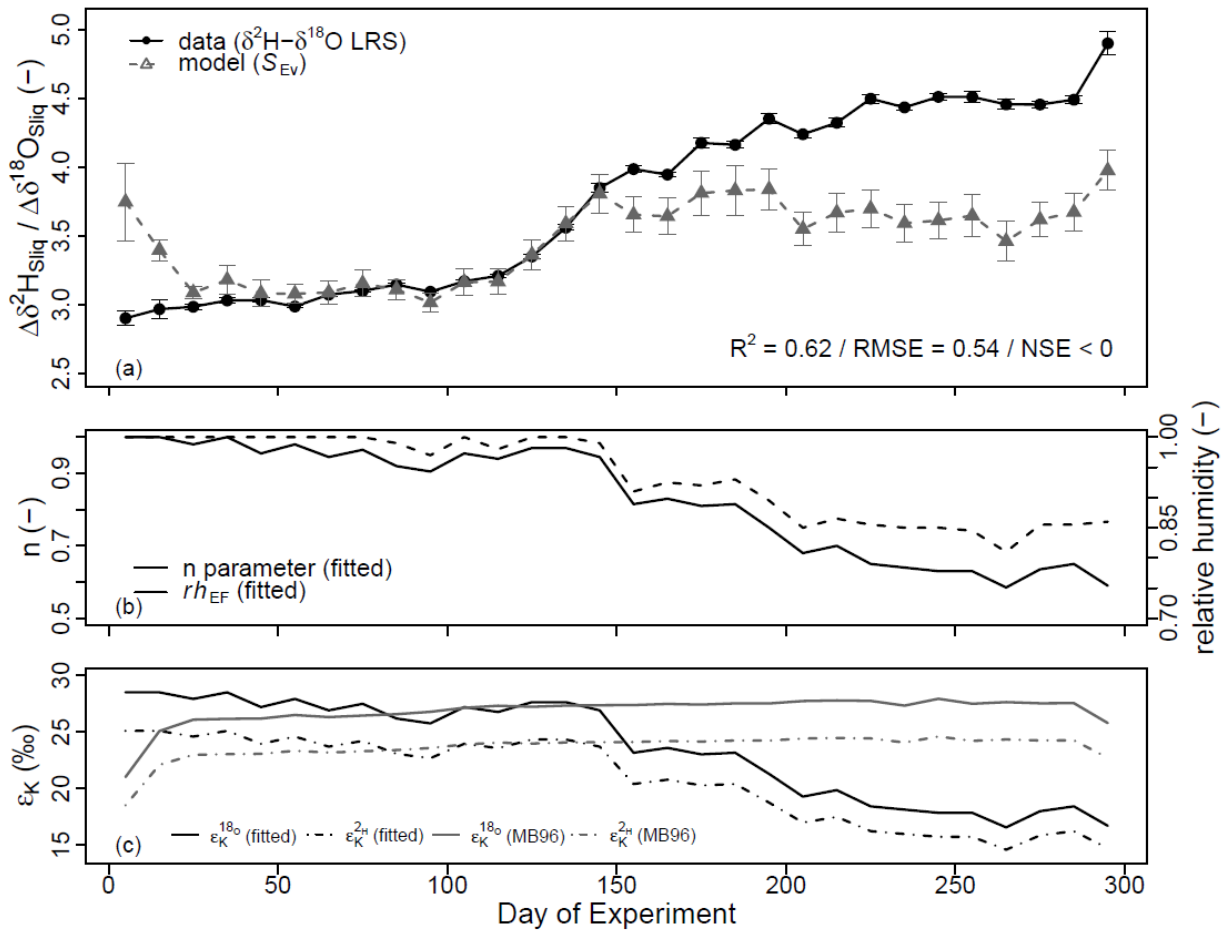
Figure 9. (a) Comparison between soil liquid water $\delta^{18}O$-δ^2H linear regressions slopes (LRS, solid black line) calculated for time intervals of ten consecutive days and simulated time series of evaporation line slope (S_{Ev}, dotted gray line) obtained from Equations (3-6) (Gat et al., 1971, Merlivat, 1978, Mathieu and Bariac, 1996). Black error bars give the standard errors of the estimated $\delta^{18}O$-δ^2H LRS. Gray error bars are the standard errors associated with calculation of S_{Ev} following Phillips and Gregg (2001). Coefficient of determination (R^2), Root Mean Square Error (RMSE) and Nash and Sutcliffe Efficiency (NSE) between model and data are reported. (b) Time series of n parameter (Eq. (6)) and soil relative humidity at the Evaporation Front (rh_{EF}) that provided the best model-to-data fit. (c) ε_K^{2H} and ε_K^{18O} time series obtained from fitted n values ("fitted") and calculated following Mathieu and Bariac (1996) ("MB96")